J Syst Eng (1995)5:192–204

Journal of Systems Engineering

Robust Nonlinear Control System Synthesis Method for Electro-Mechanical Pointing Systems with Flexible Modes

James H. Taylor* and Jin Lu†

*Department of Electrical Engineering, University of New Brunswick, Fredericton, Canada
†Odyssey Research Associates, Inc., New York, USA

A novel technique for designing robust nonlinear control algorithms for an electro-mechanical pointing system (a surrogate gun-turret testbed called the ATB1000) is presented. This system poses a very challenging control problem, as aiming accuracy must be achieved in an operational environment characterised by high-level disturbances (e.g., gun recoil) and with severe limitations imposed by the nonlinear behaviour of the drive train and the existence of flexible modes in the gun barrel.

The control synthesis approach includes two steps:

- *use of a linear control method to design a dissipative outer-loop control law to make the overall system insensitive to the unmodelled dynamics and parameter imprecision associated with the flexible modes of the wheel–barrel subsystem;*
- *use of a set of sinusoidal-input describing function (SIDF) models of the testbed's drive subsystem (which characterises the amplitude-dependent effects of backlash and nonlinear friction) to design an inner-loop nonlinear compensator to make the controlled drive-system response insensitive to input amplitude.*

This approach represents a major extension of previous SIDF-based techniques that make them applicable to systems with flexible modes. It achieves robustness in two senses: The final system is insensitive to the pointing command input amplitude and to the existence of unmodelled dynamics.

Final manuscript received 23 June 1994.
Correspondence and offprint requests to: J.H. Taylor, Department of Electrical Engineering, University of New Brunswick, PO Box 4400, Fredericton, NB Canada E3B 5A3.

Keywords: nonlinear control systems, describing functions, control system design, electro-mechanical systems, flexible mode control

1. Introduction

This paper describes the design of a robust control system for an electro-mechanical gun-turret testbed called the ATB1000, depicted schematically in Fig. 1. This testbed is used to emulate the dynamics of a gun-firing platform and to test schemes for controlling and stabilising the gun-firing process in the presence of uncertainties such as friction, backlash, flexible modes, and gun recoil disturbances.

Our control objectives are to obtain good transient response as the gun is slewed towards a specified reference angle and to maintain accurate pointing during gun firing. To achieve this level of performance, the controller must overcome the effects of gun recoil, nonlinear friction, and backlash. Furthermore, the control system is required to be robust to modelling uncertainties, such as parameter imprecision and unmodelled dynamics.

The testbed system can be decomposed into two subsystems that pose significantly different control problems. The drive subsystem has limitations due to Coulomb friction and gear backlash, and the wheel–barrel subsystem has the 'spill-over' problem associated with unmodelled high-frequency modes that arise in characterising the motion of the flexible gun barrel. The control system described below incorporates an inner-loop nonlinear control scheme based on sinusoidal-input describing function (SIDF) models to reduce the effects of backlash and nonlinear friction, and an outer-loop dissipative

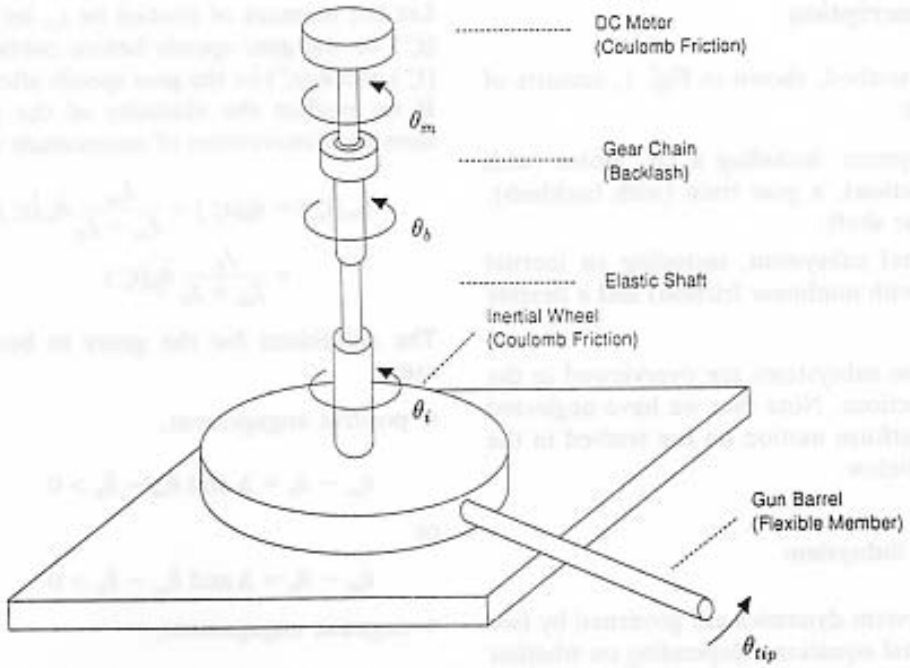

Fig. 1. Schematic of the ATB1000 electro-mechanical testbed.

control scheme to make the control system insensitive to the unmodelled dynamics and parameter imprecision of the wheel–barrel subsystem.

Both the nonlinear effects and the flexibility of the barrel are important factors in limiting the performance of the overall system. The nonlinearities in the drive subsystem make it difficult to control small motions of the gun, and the flexible modes cause large, lightly damped oscillations in the tip angle that are aggravated by 'jerky' motions due to discontinuities in the drive. To appreciate the importance of the flexible modes, we observe that the flexible member on the ATB1000 resembles a metre-long fishing rod; movies of the actual gun system show bullets being 'sprayed' as though by a high-pressure hose held some distance from the nozzle.

The nonlinear effects present in this system make the control objective for transient response difficult to meet. Robust linear control schemes [1–3] have limited utility, because they do not allow for the accommodation of amplitude dependence. This is most vividly illustrated in earlier applications of the SIDF approach [4,5] where the plant included saturation effects and stiction – the negative effects of saturation could be alleviated by using low-gain controls, while reducing the effect of stiction calls for high-gain control; the SIDF controller (which is inherently nonlinear) can accommodate these conflicting requirements, while linear control cannot.

The issue of robustly controlling semi-rigid/flexible structures has been studied intensively in recent years. For example, collocated controllers, being energy dissipative, guarantee the stability of semi-rigid/flexible structures with unmodelled modes and parametric uncertainty [6]. Being merely stabilising controllers, however, they may not simultaneously achieve desired dynamic performance [7]. As a result, non-collocated robust controllers have been used to control semi-rigid/flexible structures [8,9]. Unlike collocated controllers, many non-collocated controllers do not take into account the special structure of the controlled system which may otherwise allow better results [8]. In contrast, the outer-loop dissipative control scheme used to control the flexible wheel–barrel subsystem of the ATB1000 is a non-collocated control scheme that takes into account its special structure.

The remainder of this paper is organised as follows. In Section 2 we describe the testbed model and highlight some of the features of the system that make its control difficult; in Section 3 we formulate the control problem; in Sections 4 and 5 we detail the design of a robust control system for the testbed; finally, in Section 6, we verify the control system's performance by simulating it in conjunction with the testbed model.

2. Model Description

The ATB1000 testbed, shown in Fig. 1, consists of two subsystems:

- a drive subsystem, including a DC motor (with Coulomb friction), a gear train (with backlash), and an elastic shaft;
- a wheel–barrel subsystem, including an inertial wheel (also with nonlinear friction) and a flexible gun barrel.

Models for these subsystems are overviewed in the following subsections. Note that we have neglected the effect of platform motion on the testbed in the work outlined below.

2.1. The Drive Subsystem

The drive subsystem dynamics are governed by two sets of differential equations, depending on whether the gears are engaged or not. When the two gears are not engaged, there is no interaction between the DC motor and the elastic shaft, and thus the drive subsystem is composed of two decoupled second-order differential equations:

$$J_m\ddot{\theta}_m = T_m - T_{mf} \tag{1}$$

$$J_b\ddot{\theta}_b = -T_s \tag{2}$$

where θ_m and θ_b are the angles of the driving gear and driven gear, respectively (see Fig. 1). J_m and J_b are the inertia constants of the motor and elastic shaft assemblies, T_m is the mechanical torque produced by the motor, T_{mf} is the Coulomb friction torque on the motor

$$T_{mf} = b_m \operatorname{sgn}(\dot{\theta}_m)$$

where b_m is the magnitude of the friction torque, and T_s is the reactive torque of the elastic shaft,

$$T_s = k_s(\theta_b - \theta_i) + b_s(\dot{\theta}_b - \dot{\theta}_i) \tag{3}$$

where k_s and b_s are spring and viscous friction constants respectively, and θ_i is the inertial wheel yaw angle.

When the two gears are engaged, the subsystem can be treated as if there were no gears. In this case, $\dot{\theta}_m = \dot{\theta}_b$ and $\theta_m = \theta_b + \Delta$ (positive engagement) or $\theta_m = \theta_b$ (negative engagement), where Δ is the backlash gap. Under these circumstances, the differential equation governing the dynamics of θ_b is

$$(J_m + J_b)\ddot{\theta}_b = T_m - T_s - T_{mf} \tag{4}$$

We note that there is a 'jump' in the states $\dot{\theta}_m$ and $\dot{\theta}_b$ at the moment the two gears become engaged. Let the moment of contact be t_c, let $\dot{\theta}_m(t_c^-)$ and $\dot{\theta}_b(t_c^-)$ be the gear speeds before contact, and let $\dot{\theta}_m(t_c^+)$ and $\dot{\theta}_b(t_c^+)$ be the gear speeds after engagement. If we neglect the elasticity of the gear material, then by conservation of momentum we have

$$\dot{\theta}_m(t_c^+) = \dot{\theta}_b(t_c^+) = \frac{J_m}{J_m + J_b}\dot{\theta}_m(t_c^-) + \frac{J_b}{J_m + J_b}\dot{\theta}_b(t_c^-) \tag{5}$$

The conditions for the gears to become engaged are:

- positive engagement,

$$\theta_m - \theta_b = \Delta \text{ and } \ddot{\theta}_m - \ddot{\theta}_b > 0 \tag{6}$$

or

$$\theta_m - \theta_b = \Delta \text{ and } \ddot{\theta}_m - \ddot{\theta}_b > 0 \tag{7}$$

- negative engagement,

$$\theta_m - \theta_b = 0 \text{ and } \dot{\theta}_m - \dot{\theta}_b < 0 \tag{8}$$

or

$$\theta_m - \theta_b = 0 \text{ and } \ddot{\theta}_m - \ddot{\theta}_b < 0 \tag{9}$$

We note that in the above conditions, the dynamics of θ_m and θ_b are governed by differential equations (1) and (2).

The conditions under which the gears become disengaged are more complicated to state in terms of simple tests on angles or angle rates. The most straightforward technique, used here, is to continue to evaluate $\ddot{\theta}_m$ and $\ddot{\theta}_b$ according to Eqs (1), (2) with current values of $\theta_m = \theta_b + \Delta$ (positive engagement) or $\theta_m = \theta_b$ (negative engagement); again, we have two cases:

- positive engagement – the gears will disengage when Eqs (1), (2) predict that $\dot{\theta}_b > \dot{\theta}_m$;
- negative engagement – the gears will disengage when Eqs (1), (2) predict that $\dot{\theta}_b < \dot{\theta}_m$;

Prior to such an event, the dynamics obey the differential equation (4).

2.2. The Wheel–Barrel Subsystem

The gun barrel is a distributed-parameter system that can be approximated by a lumped-parameter model obtained using the finite element method. After this approximation, the wheel–barrel subsystem is described by a state-space model of the following form:

$$\ddot{x} + D\dot{x} + Kx = B(T_s - T_g + T_{f1} + T_{f2}) \tag{10}$$

$$y = Cx \tag{11}$$

where $x \in \mathcal{R}^n$ is the subsystem state vector (vector of modal coordinates) and $y^T = [\theta_i \ \theta_{tip}]$ is the output vector; θ_i is the inertial-wheel angle and θ_{tip} is the gun-barrel tip-angle; and matrices D, K, C and B are of appropriate dimensions. The arrays D and K are diagonal matrices with non-negative elements. T_g is the disturbance torque introduced by gun firing (recoil), and T_{f1} and T_{f2} are torques introduced by viscous and Coulomb friction between the inertial wheel and the supporting platform under it,

$$T_{f1} = b_1\dot{\theta}_i \tag{12}$$

$$T_{f2} = b_2\,\mathrm{sgn}(\dot{\theta}_i) \tag{13}$$

where b_1 and b_2 are the friction coefficients.

The dimension of a flexible-structure model (in a lumped-parameter approximation) is generally quite high. From a numerical standpoint, we usually base the design of a controller for a flexible structure on a reduced-order model that contains the critical modes of the structure. In our case, we consider only four low-frequency modes of the wheel–barrel structure ($n = \dim(x) = 4$ in Eq. (10)). One important issue is how to design a control law based on the reduced-order model that does not destabilise the unmodelled modes when applied to the actual system.

3. Control Problem Statement

The objectives of the control system are to slew smoothly and point accurately the gun-barrel tip-angle θ_{tip} with respect to a reference angle (pointing command input) in the presence of gun-firing disturbances, backlash, nonlinear friction, and unmodelled dynamics. To be specific, we want to find a control law $T_m = T_m(t)$ such that θ_{tip} will slew gracefully to θ_{ref} within some acceptable tolerance and in a reasonable time. To achieve this control objective, the control system must overcome the effect of backlash (the DC motor has no control over the wheel–barrel subsystem during disengagement) and Coulomb friction (the torques are discontinuous whenever angular velocity changes sign, giving rise to jerky motion and ringing). In addition, the control system is required to be insensitive to modelling uncertainty, such as unmodelled high-frequency modes and system parameter imprecision of the flexible gun barrel.

Substituting relations (3) and (12) into Eq. (10), we can write the model of the wheel–barrel subsystem as

$$\ddot{x} + (D + (b_s + b_1)BC_1)\dot{x} + (K + k_sBC_1)x = Bu + Bw \tag{14}$$

where $\theta_i = C_1x$ and C_1 is the first row of C in Eq. (11), $u = b_s\dot{\theta}_b + k_s\theta_b$, and $w = T_g + T_{f2}$.

The variable $u = b_s\dot{\theta}_b + k_s\theta_b$ can be considered to be the input to the system in Eq. (14) and an output of the drive subsystem. Our approach to control design consists of two steps.

1. Find a control law u^d for the input u to the system in Eq. (14) such that the resulting θ_{tip} has the desired properties outlined above.
2. Find a control law for T_m so that u as an output of the drive subsystem tracks the desired control law u^d found in Step 1.

This design approach is illustrated in Fig. 2, where the linear controller $C_L(s)$ is designed in Step 1 and the nonlinear controller C_{NL} is designed in Step 2. In Step 1, we will use a robust linear control scheme that does not destabilise unmodelled high-frequency modes and is insensitive to parameter uncertainty. In Step 2, we will use a nonlinear control synthesis approach based on SIDF models of the testbed's drive subsystem to deal with backlash and nonlinear friction. SIDF models are used because they provide a meaningful characterisation of the major nonlinear effect of the drive subsystem with which we are concerned: the sensitivity of the drive subsystem's input–output (IO) behaviour to the amplitude of the input signal due to the amplitude-dependent behaviour of gear backlash and Coulomb friction.

4. Robust Control of the Wheel–Barrel Subsystem

Consider a constant linear feedback control law for the system in Eq. (14):

$$u = -F_1\dot{x} - F_2x \tag{15}$$

where F_1 and F_2 are two feedback gain matrices of suitable dimension.

Substituting Eq. (15) into Eq. (14) yields

$$\ddot{x} + (D + (b_s + b_1)BC_1 + BF_1)\dot{x} + (K + k_sBC_1 + BF_2)x = Bw \tag{16}$$

We note that $C_1 = [c_{11} \ldots c_{1n}]$ ($\theta_i = C_1x$) and $B = [b_1 \ldots b_n]^T$ in the model in Eq. (16) has the relation $c_1b_i > 0$, $i = 1, \ldots, n$. In fact, the viscous bearing torque $T_{f1} = b_1\dot{\theta}_i = b_1C_1\dot{x}$. If we assume that the wheel–barrel subsystem is subject only to the viscous bearing torque and has natural damping $D = 0$, then we have from Eq. (10),

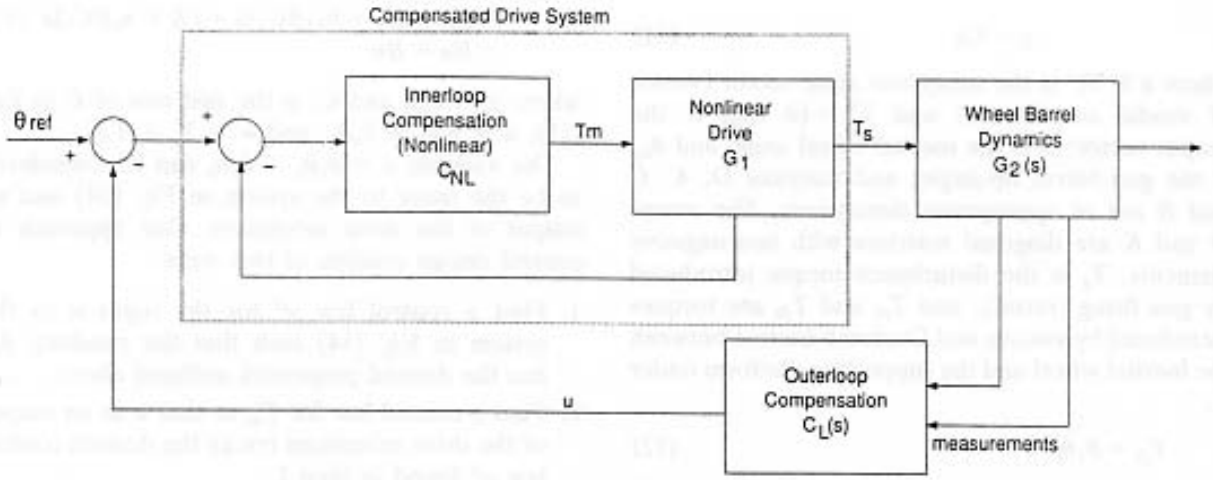

Fig. 2. Block diagram for the nonlinear control system.

$$\ddot{x} + Kx = -BT_{f1} = -BC_1\dot{x} \tag{17}$$

We know that a system with only viscous bearing torque is always energy dissipative. For the system in Eq. (17), this is true if and only if $c_{1i}b_i > 0$, $i = 1, \ldots, n$.

The following results give sufficient conditions for the system in Eq. (16) to be stable; refer to [10] for proofs.

Proposition 1. Assume the diagonal matrices D and K satisfy $\text{rank}(D) \geq n - 1$ and $\text{rank}(K) \geq (n - 1)$. Then the system in Eq. (14) with the control law in Eq. (15) is asymptotically stable if $F_1 = f_1C_1$ and $F_2 = f_2C_1$ with scalars $f_1 \geq 0$ and $f_2 \geq 0$ (in other words, $u = f_1\dot{\theta}_i + f_2\theta_i$).

We note that there is a theorem similar to the result of Proposition 1 for a simpler controller under the assumption of zero natural damping [11].

In the following result, we neglect the damping in the system in Eq. (14), since a control law that stabilises this system with zero natural damping will stabilise it with positive natural damping.

Proposition 2. Let the damping matrix D in the system in Eq. (14) be zero and the diagonal matrix K satisfy $\text{rank}(K) \geq (n - 1)$. The system in Eq. (14) with the control law in Eq. (15) is asymptotically stable if $F_1 = f_1C_1 + f_3[1\ 0\ \ldots\ 0]$ and $F_2 = f_2C_1$ with scalars $f_1 \geq 0$, $f_2 \geq 0$ and $f_3 \geq 0$ (in other words, $u = f_1\dot{\theta}_i + f_3\dot{x}_1 + f_2\theta_i$).

Propositions 1 and 2 define control schemes that are robust with respect to system modelling errors and structural perturbations, because their stability depends on system parameter *signs*, not values.

In the sequel, we will consider only the control scheme

$$u = f_1\dot{\theta}_i + f_2\theta_i + f_3\dot{x}_1 \tag{18}$$

where $f_i \geq 0$, $i = 1, 2, 3$. The freedom in choosing f_i's in the control scheme allows us to achieve other performance requirements such as desirable pole assignment while ensuring the stability of the system.

5. SIDF Control Synthesis for the Drive Subsystem

Assume that we have found, for the wheel–barrel subsystem in Eq. (14), the control law for $u = b_s\dot{\theta}_b + k_s\theta_b$ which guarantees the required behaviour of θ_{tip}. Now, we will design a nonlinear control algorithm based on SIDF models of the drive subsystem such that $u = b_s\dot{\theta}_b + k_s\theta_b$ as an output of the drive subsystem matches this desired behaviour.

5.1. SIDF Modelling of the Drive Subsystem

There are two approaches to generating SIDF models for the drive subsystem from input T_m to desired output $u = b_s\dot{\theta}_b + k_s\theta_b$ [12].

1. Develop a state-space model of the subsystem in which every nonlinear element is replaced analytically by the corresponding scalar SIDF, formulate the equations of harmonic balance, select an input amplitude a ($T_m(t) = a\ \sin(\omega t)$), solve for the unknown amplitudes of the state variables and scalar SIDF values, and compute the IO model as

$$G(j\omega,a) = C(a)[j\omega I - A(a)]^{-1}\,B(a) + D(a)$$

where we stress that all arrays in the quasilinear

model may depend on the input amplitude a. We did not use this approach for this effort, so we merely refer to [13] for further details.

2. Apply a sinusoidal signal $T_m = a \sin(\omega t)$ to the drive subsystem model, perform direct Fourier integration of the drive subsystem output $u = b_s\dot{\theta}_b + k_s\theta_b$ in parallel with simulating the model's response to the sinusoidal input, and simulate until steady-state is achieved to obtain $G(j\omega,a)$ [14].

To elaborate on the second method and illustrate its use on the ATB1000, we specified a range of input amplitudes $[a_{\min},a_{\max}]$ to cover the expected operating range of the servo motor and frequencies $[\omega_{\min},\omega_{\max}]$ to span the frequency range required for control system design. Then specific sets of values $\{a_i\} \in [a_{\min},a_{\max}]$ and $\{\omega_j\} \in [\omega_{\min},\omega_{\max}]$ were selected for generating $G(j\omega_j,a_i)$. The ATB1000 simulation model was augmented by adding new 'state variables' corresponding to the Fourier integrals

$$\mathrm{Re}(G_K(j\omega_j,a_i)) = \frac{\omega_j}{\pi a_i}\int_{t_0+KT}^{t_0+(K+1)T} y(t)\sin(\omega_j t)\,\mathrm{d}t \tag{19}$$

$$\mathrm{Im}(G_K(j\omega_j,a_i)) = \frac{\omega_j}{\pi a_i}\int_{t_0+KT}^{t_0+(K+1)T} y(t)\cos(\omega_j t)\,\mathrm{d}t \tag{20}$$

where $\mathrm{Re}(\cdot)$ and $\mathrm{Im}(\cdot)$ are real and imaginary parts of the SIDF $G(j\omega_j,a_i)$, $T = 2\pi/\omega_j$, and $y(t)$ is the output of the nonlinear drive subsystem. Achieving steady state for a given a_i and ω_j was guaranteed by setting certain tolerances and convergence criteria on $\mathrm{Re}(G_K)$ and $\mathrm{Im}(G_K)$ where K corresponds to the number of cycles simulated; the integration is interrupted at the end of each cycle and the convergence criteria checked to see if the results were within tolerance so that the simulation could be stopped and $G(j\omega_j,a_i)$ reported. For further detail, refer to [14,15].

For linear systems, such a model is independent of input amplitudes; in fact, it is the usual transfer function $G(j\omega)$. For nonlinear systems, however, SIDF models generally depend on the amplitude of the system input. This is demonstrated in Fig. 3, which portrays the amplitude-dependent frequency response for the drive subsystem. Observe that for the smallest amplitude the result $|G(j\omega_j,a_i)|$ is erratic for ω_j beyond 1 rad s^{-1}; this is due to the fact that for small input amplitudes the gear backlash is barely transmitting torque to the wheel. As the amplitude increases the frequency response is clearly converging; this is because backlash and Coulomb friction have decreasing impact as the range of motion increases, and in fact $G(j\omega_j,a_i)$ approaches the linear approximation obtained by neglecting these effects altogether as a_i increases.

5.2. SIDF Control Algorithm Synthesis

The goal of the SIDF synthesis procedure is to generate a nonlinear control law in the following 'nonlinear proportional-integral-derivative (PID)' form:

$$T_m = f_P(e) + \int_0^t f_I(e)\,\mathrm{d}t + \frac{\mathrm{d}}{\mathrm{d}t}f_D(e) \tag{21}$$

where T_m (the motor input) is the output of the controller, $e = \theta_{\mathrm{ref}} - u$ with θ_{ref} an external input (see Fig. 2), and $f_P(\cdot)$, $f_I(\cdot)$ and $f_D(\cdot)$ are nonlinear functions to be obtained by an amplitude-desensitisation process involving SIDF inversion. There are several variants of the SIDF synthesis approach; we summarise below the specific approach applied to the ATB1000 [4]. For a detailed description of other SIDF-based control design methods, see also [5,16].

The procedure applied to the ATB1000 involves seven steps.

1. Select a set of plant operating regimes defined by sets of input amplitudes $\{a_i\}$ and frequencies $\{\omega_j\}$ as outlined above and generate the corresponding SIDF models $G_{i,j} = G(j\omega_j,a_i)$.
2. Select one plant operating amplitude from this set, denoted by $a^* \in [a_{\min},a_{\max}]$ and characterised by $G^*(j\omega,a^*)$.
3. Design a linear PID controller denoted $C^*(j\omega)$ based on $G^*(j\omega; a^*)$ using some classical frequency-domain method (e.g., design to achieve good bandwidth and gain-margin).
4. Use $C^*(j\omega)$ and $G^*(j\omega; a^*)$ to define an *achievable open-loop objective function* denoted $C\,G^*(j\omega)$.
5. Take the SIDF model data points $G_{i,j}$ and error-signal amplitude set $e_k, k = 1, 2, \ldots$ and for each k determine the linear compensator static gains $K_{P,k}$, $K_{I,k}$, $K_{D,k}$ required to force the frequency response of the PID followed by $G_{i,j}(j\omega_j;\ a_k)$ where $a_k = (K_{P,k} + K_{I,k}/j\omega_j + j\omega_j K_{D,k})\,e_k$ to fit the open-loop objective function $C\,G^*(j\omega)$ with minimum mean-square error.
6. Pass the three gain sets $K_{P,k}(e_k)$, $K_{I,k}(e_k)$, $K_{D,k}(e_k)$ to an SIDF inversion routine [14] for controller nonlinearity synthesis.
7. Validate the nonlinear controller design by evalu-

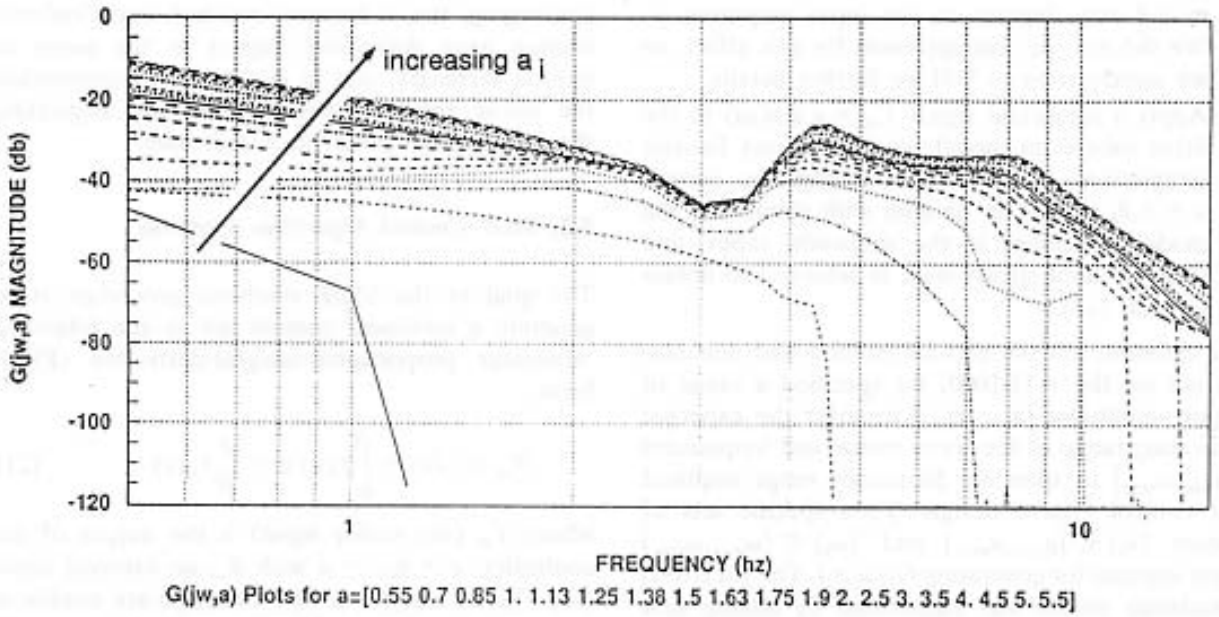

Fig. 3. Frequency-response plots for the drive subsystem.

ating its open-loop frequency response (SIDF models as above) and by closed-loop transient-response simulation.

Steps 2–4 result in an 'achievable open-loop objective function' in the sense that $C\,G^*$ is based on an actual plant characterisation and PID controller. The plant characterisation could as well be a linearised plant transfer function instead of an SIDF model for a particular amplitude, although neglecting nonlinear effects altogether might be unwise in some circumstances. Also, there are many ways in which $C\,G^*$ may be determined, including picking an open-loop transfer function simplistically based on classical linear control ideas (e.g., select it based on a second-order approximation with desired natural frequency and damping ratio). Unless the designer has a good idea of what is achievable, the latter approach might prove to be inadvisable.

The SIDF inversion approach used in Step 6 is rather different from the classical problem and its (limited) solution (see Section 3.7 of [17]). In the general analytical case, a single-valued nonlinearity may be expressed as the solution to a Volterra integral equation of the first kind. However, in most cases this cannot be solved, and where it can, different SIDFs may give rise to the same nonlinearity. In the special case of polynomial nonlinearities, the coefficients of the nonlinearity can be obtained directly from those of the SIDF – however, in this application we have a small number of gain–amplitude values that are obtained empirically (not in relation to any actual nonlinearity), so this would very likely be a dangerous procedure. There are several pitfalls: first, the gain–amplitude data would have to be fitted with a polynomial, and in many cases the fit will not be good; secondly, implementing a higher-order polynomial in the controller may be ill-advised, since the behaviour of the nonlinearity outside the fitting range may be extremely adverse (e.g., destabilising).

In contrast to these approaches, we select a class of piece-wise linear functions (which are easily implemented and parsimoniously parameterised), and simply obtain the best fit to the gain–amplitude values obtained in Step 5 by adjusting the nonlinearity parameters to minimise mean-square error, and thus achieve the desired reduction in amplitude sensitivity of the open-loop frequency response. Synthesis of the drive-system controller was done using the nonlinearity class depicted in Fig. 4; it is described by four parameters, can fit a wide variety of gain–amplitude relationships (e.g., monotone increasing, monotone decreasing, concave up, concave down), and is linear for large values of amplitude. This method appears to be very robust.

This approach results in designing a nonlinear control system whose open-loop frequency response has as little amplitude sensitivity as possible given the 'degrees of freedom' inherent in the PID control algorithm. The power of this approach can be appreciated by observing that the independent synthesis of the nonlinearities $f_P(\cdot)$, $f_I(\cdot)$ and $f_D(\cdot)$ in

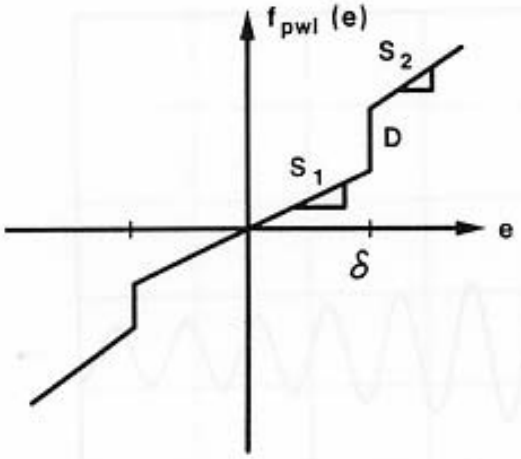

Fig. 4. Nonlinearity class for SIDF inversion.

Eq. (21) allows for desensitisation at low frequencies (via f_I), middle frequencies (via f_P) and high frequencies (via f_D). This frequency-domain insensitivity appears, on the basis of a number of applications, to minimise transient response sensitivity as well. Note that the fact that the amplitude-dependent frequency responses are forced to match a conservative frequency-domain characteristic should afford a good degree of robustness with respect to parameter uncertainly as well; since the drive-train nonlinearity parameters are rather precisely known (in comparison with those in the modal model) we did not test for this aspect.

6. Design and Simulation Study

The parameters of the testbed system are listed in Table 1. The dynamic response of θ_{tip} of the open-loop testbed system in response to a non-zero initial condition ($\theta_{tip} \neq 0$), and in the presence of friction, backlash, and gun-firing disturbance, is shown in Fig. 5. From Fig. 5, we see that the modes of the barrel are quite lightly damped. We found that the damping ratio of the lowest-frequency mode is about 10%, and the damping ratios of other modes are less than 10%. Therefore, we use the degrees of freedom in Eq. (18) to increase the damping of the two lowest-frequency modes. Using any pole assignment method (for example, see [18]) we find that when $u = -3.5\dot{x}_1 - 10\theta_i$ the damping ratios of the first- and second-lowest-frequency modes are 40% and 20% respectively. By Proposition 2, the control scheme guarantees the stability of the system.

The SIDF-based control nonlinearities obtained in Step 6 for the drive subsystem control algorithm in Eq. (21) are shown in Fig. 6. Figure 7 portrays a set of SIDF models (frequency responses) of the open-loop nonlinear compensated drive subsystem – we observe that the variation of magnitude is greatly reduced compared with the results for the drive train alone (Fig. 3); the same is true for phase.

Figure 8 shows the uniformly fast response of $u = b_s\dot{\theta}_b + k_s\theta_b$ of the drive subsystem controlled by the nonlinear algorithm when subjected to step inputs of various amplitudes. For comparison, Fig. 9 shows the response of $u = b_s\dot{\theta}_b + k_s\theta_b$ of the drive subsystem controlled by a linear algorithm (design based on a linearised model of the testbed) when excited by step inputs with the same set of amplitudes. Figure 9 also includes the response of $u = b_s\dot{\theta}_b + k_s\theta_b$ of the *linearised* model controlled by the linear control system. As mentioned earlier,

Table 1. Parameters of the ATB1000.

Symbol	Description	Value	Units
Δ	Backlash clearance	0–0.05	rad
b_s	Spring viscosity	0.1	Nm rad^{-1} s^{-1}
k_s	Spring constant	34.3	Nm rad^{-1}
b_m	Motor friction magnitude	0.5	Nm
J_m	Motor and driving gear inertia	0.006	Kg m^2
J_b	Driven gear and shaft intertia	0.01	Kg m^2
b_1	Bearing viscosity	0.67	Nm rad^{-1} s^{-1}
b_2	Inertial wheel friction magnitude	0.1	Nm
D	Damping matrix	diag([0 0.891 4.08 11.35])	Nm rad^{-1} s^{-1}
K	Stiffness matrix	diag([0 912.5 19124 148,155])	Nm rad^{-1}
B^T	Input gain vector	[5.7 27.6 −17.1 −14.9]	
C	Output matrix	$\begin{bmatrix} 1.28 & 0.316 & -0.063 & -0.015 \\ 1.28 & -0.798 & -1.45 & 1.23 \end{bmatrix}$	

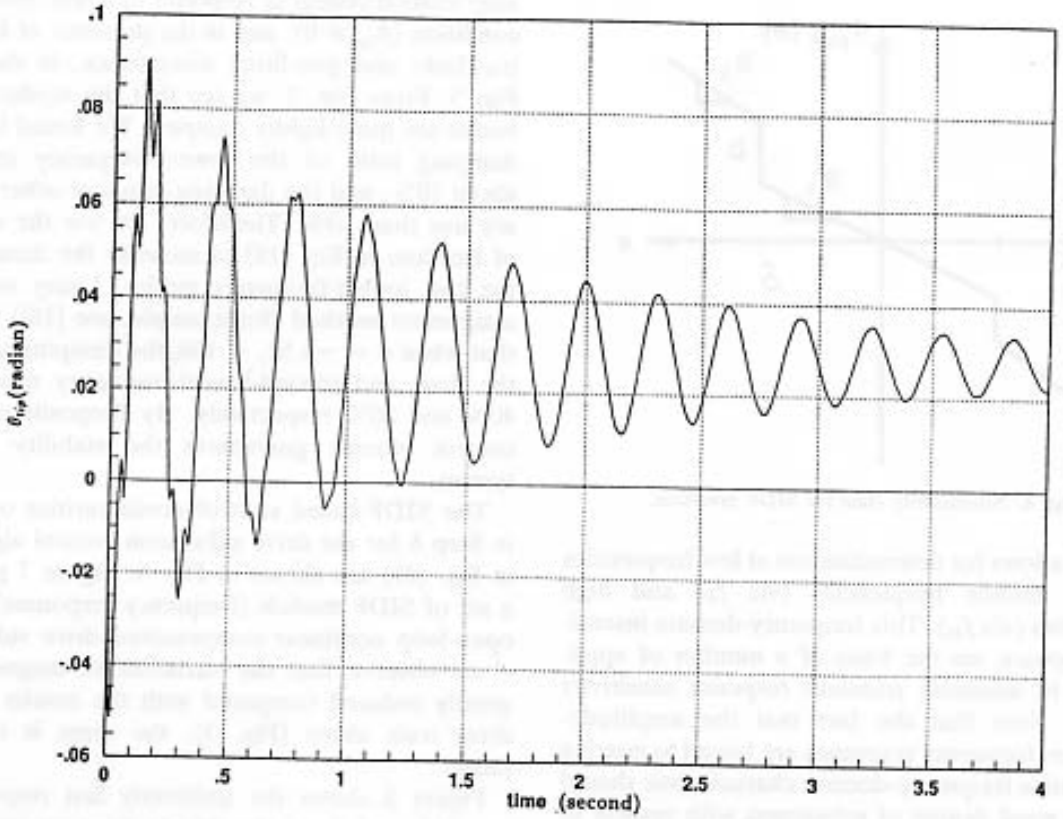

Fig. 5. Open-loop response of θ_{tip}.

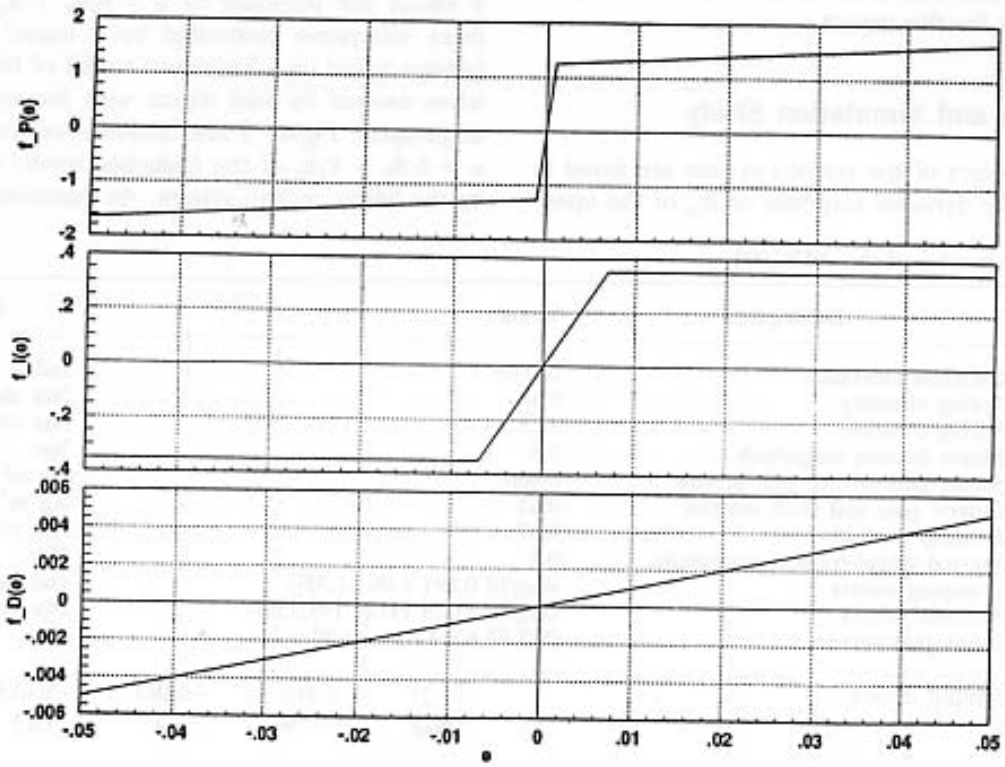

Fig. 6. Controller nonlinearities obtained via SIDF inversion.

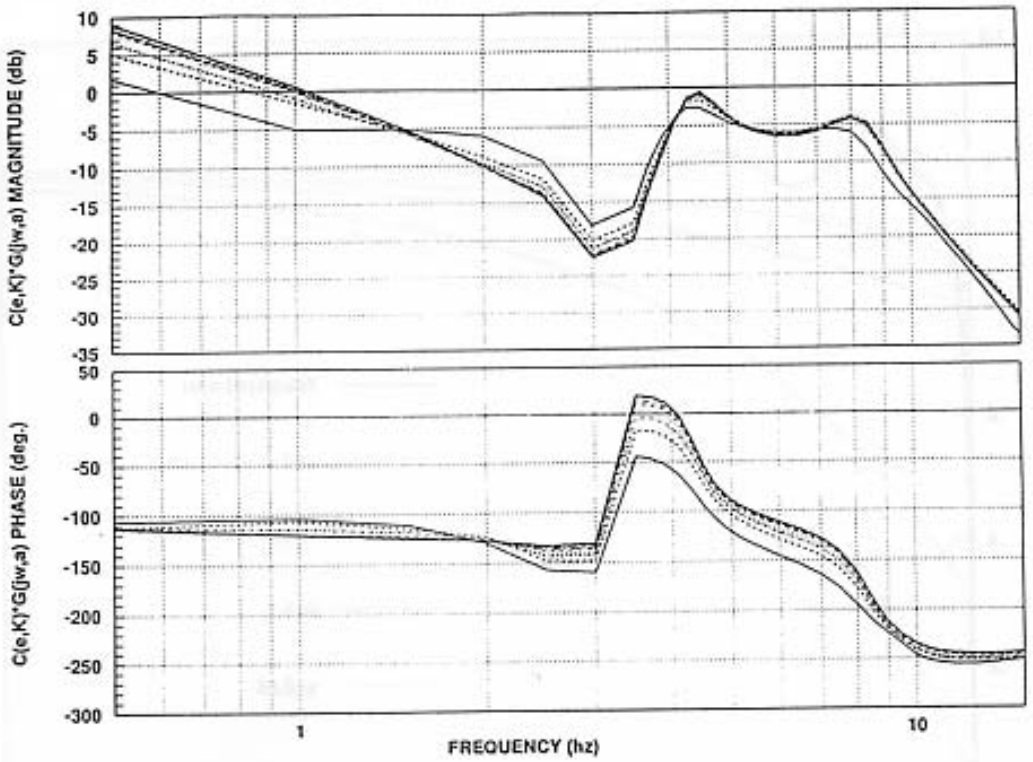

Fig. 7. Open-loop frequency-response plots for the nonlinear compensated drive subsystem.

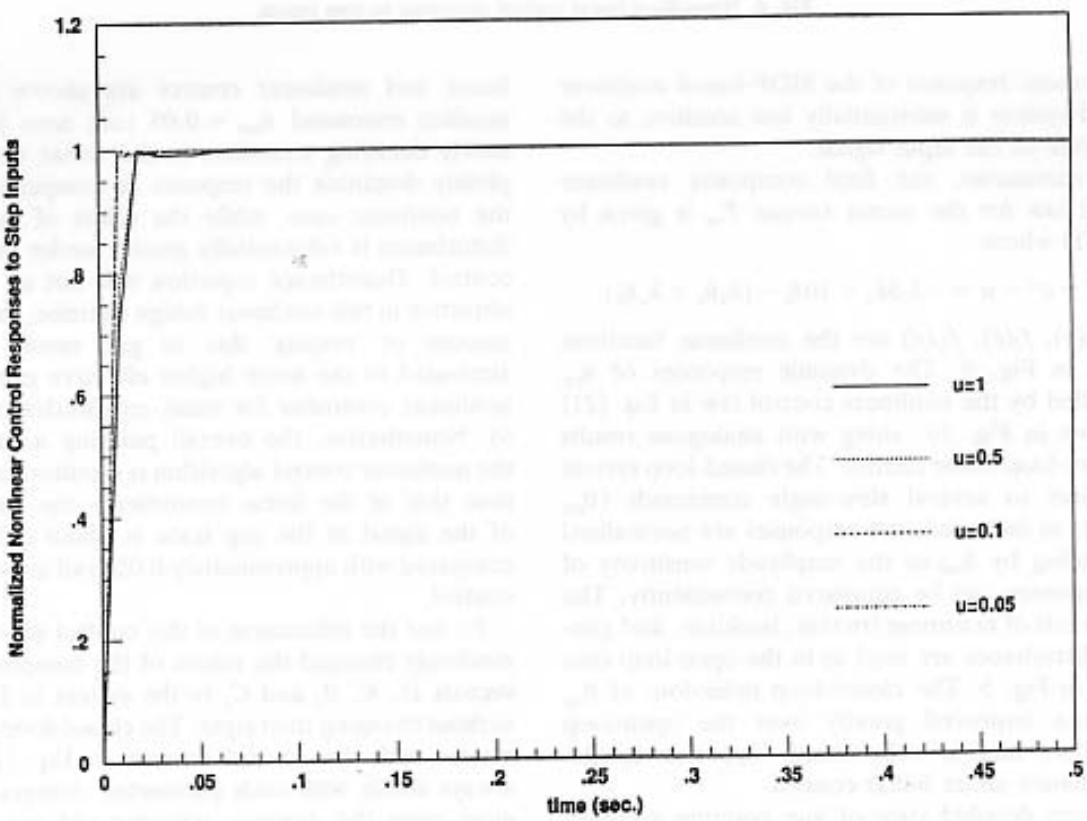

Fig. 8. Normalised nonlinear control responses to step inputs.

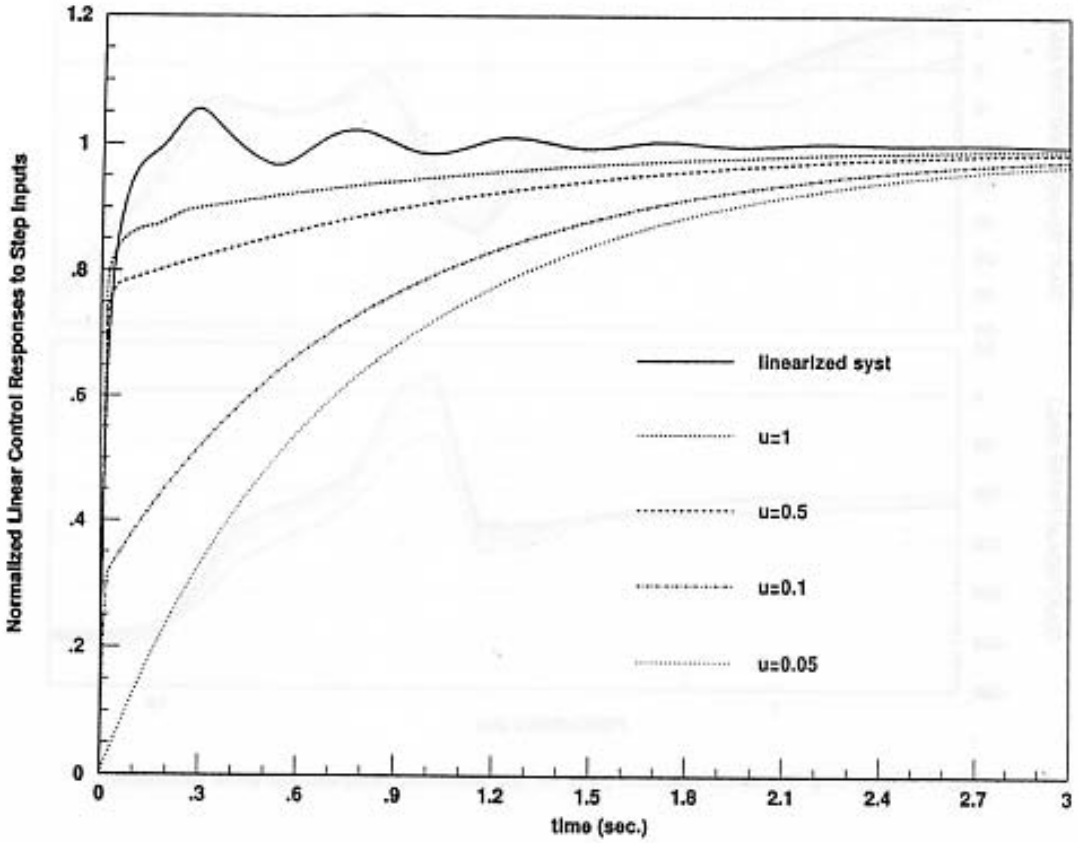

Fig. 9. Normalised linear control responses to step inputs.

the dynamic response of the SIDF-based nonlinear control system is substantially less sensitive to the amplitude of the input signal.

To summarise, the final composite nonlinear control law for the motor torque T_m is given by Eq. (21) where

$$e = u^d - u = -3.5\dot{x}_1 - 10\theta_i - (b_s\dot{\theta}_b + k_s\theta_b)$$

and $f_P(e)$, $f_I(e)$, $f_D(e)$ are the nonlinear functions shown in Fig. 6. The dynamic responses of θ_{tip} controlled by the nonlinear control law in Eq. (21) is shown in Fig. 10, along with analogous results for inner-loop linear control. The closed-loop system is subject to several slew-angle commands (θ_{ref} values), as indicated; the responses are normalised by dividing by θ_{ref} so the amplitude sensitivity of the responses can be compared conveniently. The same levels of nonlinear friction, backlash, and gun-firing disturbance are used as in the open-loop case shown in Fig. 5. The closed-loop behaviour of θ_{tip} has been improved greatly over the open-loop behaviour, and is substantially superior to the performance under linear control.

A more detailed view of gun pointing accuracy is provided in Fig. 11, where the responses with linear and nonlinear control are shown for the smallest command $\theta_{ref} = 0.05$ rad; note that the slowly decaying transients in the linear case completely dominate the response in comparison with the nonlinear case, while the effect of gun-firing disturbance is substantially greater under nonlinear control. Disturbance rejection was not an explicit objective in this nonlinear design exercise; the larger amount of 'ringing' due to gun recoil can be attributed to the much higher effective gain of the nonlinear controller for small amplitudes (see Fig. 6). Nonetheless, the overall pointing accuracy of the nonlinear control algorithm is significantly better than that of the linear controller – the amplitude of the signal in the top trace is about 0.005 rad, compared with approximately 0.012 rad under linear control.

To test the robustness of this control scheme, we randomly changed the values of the components of vectors D, K, B, and C_1 in the system in Eq. (14) without changing their signs. The closed-loop testbed system with the control scheme in Eq. (21) was always stable with such parameter changes and in most cases the dynamic response did not change noticeably.

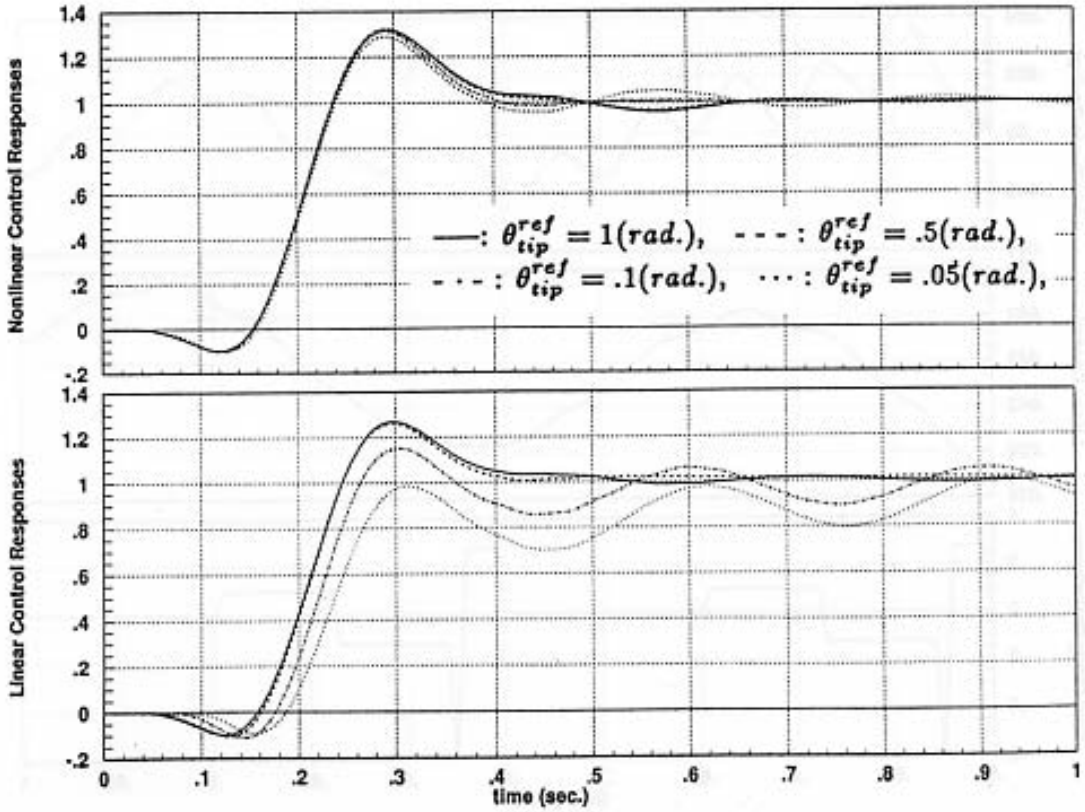

Fig. 10. Normalised nonlinear closed-loop responses to step inputs.

7. Conclusion

We have developed a nonlinear control algorithm for the ATB1000 testbed model and tested it by simulation. The control system fulfilled our performance objectives: it worked well in the presence of backlash, Coulomb friction, and gun-firing disturbances, and behaved consistently for a wide range of input command levels. The control system is robust with respect to both input amplitude and modelling uncertainties such as parameter imprecision and unmodelled dynamics of the flexible element. This development and application represent the first extension of the SIDF nonlinear control synthesis approach to encompass electro-mechanical systems with flexible modes.

Acknowledgement

Support for the research described herein has been provided by the Advanced Research Projects Agency through the US Army ARMCCOM at Picatinny Arsenal, Dover, NJ, by Contract Number DAAA21-92-C-0013.

The ATB1000 electro-mechanical pointing system was built by Integrated Systems Inc., Santa Clara, CA, for the Army Research, Development and Engineering Center (ARDEC), Picatinny Arsenal, Dover, NJ.

The ATB1000 model was also supplied by Integrated Systems Inc. to ARDEC, and modified by the authors to correct the engagement conditions and incorporate improved parameter values.

The authors would like to recognise the support and encouragement provided by Mr Mike Mattice and Dr Norm Coleman of ARDEC. Earlier controllers were successfully tested on the ATB1000 with their aid; however, the opportunity to test the present algorithm on the testbed was not available.

References

1. Doyle JC, Stein G. Multivariable feedback design: concepts for a classical/modern synthesis. IEEE Trans Autom Control 1981; AC-26(1): 4–16
2. Hung YS, MacFarlane AGJ. Multivariable feedback: a quasi-classical approach. Lecture Notes in Control and Information Sciences, vol 40, Springer-Verlag, 1982
3. Francis BA. H^{∞}-optimal feedback controllers for linear multivariable systems. IEEE Trans Autom Control 1984; AC-29(10): 888–900 (see also A course

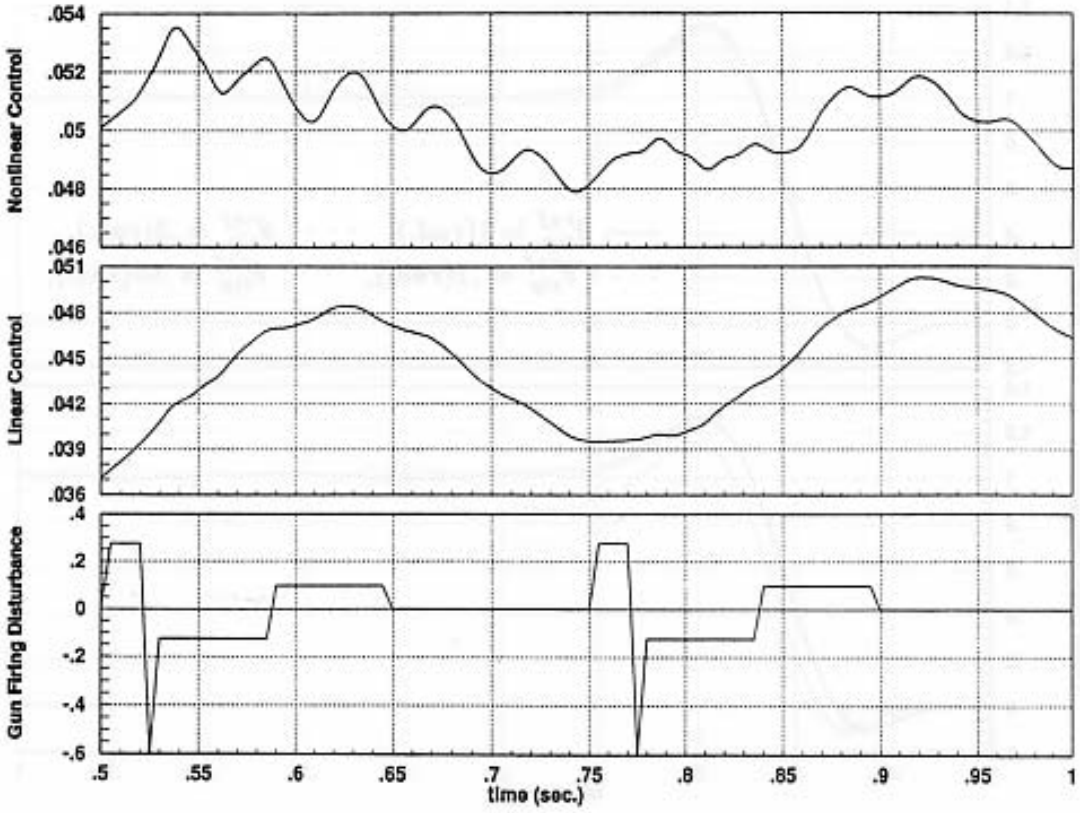

Fig. 11. Responses of θ_{tip} to gun-firing disturbance.

in H_∞ control theory, Lecture Notes in Control and Information Sciences, vol 88, Springer-Verlag, 1987)
4. Taylor JH, Strobel KL. Nonlinear compensator synthesis via sinusoidal-input describing functions. In: Proc. American control conference, Boston MA, June 1985, pp 1242–1247
5. Taylor JH, O'Donnell JR. Synthesis of nonlinear controllers with rate feedback via SIDF methods. In: Proc. American control conference, San Diego, CA, May 1990, pp 2217–2222
6. Balas MJ. Direct velocity feedback control of large space structure. J Guid Control 1979; 2: 252–253
7. Lu J, Thorp JS, Chiang H-D. Modal control of large flexible structures using collocated actuators and sensors. IEEE Trans Autom Control, 1992; 37: 143–148
8. Lim K, Maghami P, Joshi S. A comparison of controller design for an experimental structure. Proc American control conference, Boston, MA, 26–28 June 1991, pp 1343–1352
9. Buddie SA, Georgiou TT, Ozguner U, Smith MC. Flexible structure experiments at JPL and WPAFB: H_∞ controller design. In: Proc. American control conference, Chicago, IL, 24–26 June 1992, pp 1675–1680
10. Lu J. Robust control of semi-rigid/flexible structures. In: Proc. American control conference, San Francisco, CA, June 1993, pp 2882–2886
11. Gevarter WB. Basic relations for control of flexible vehicles. AIAA J 1970; 8(4): 666–672
12. Taylor JH. Robust computer-aided control system design for nonlinear plants. In: Proc. application of multivariable systems theory, Manadon, Plymouth, UK, October 1982, pp 33–40
13. Taylor JH. A systematic nonlinear controller design approach based on quasilinear system models. In: Proc. American control conference, San Francisco, CA, June 1983, pp 141–145
14. Taylor JH. Computer-aided control engineering environment for nonlinear systems analysis and design. In: Proc. third IFAC symposium on computer-aided design in control and engineering systems. Lyngby, Denmark, August 1985, pp 38–43
15. Taylor JH, Lu J. Computer-aided control engineering environment for the synthesis of nonlinear control systems. In: Proc. American control conference, San Francisco, CA, June 1993, pp 2557–2561
16. Taylor JH, Strobel KL. Applications of a nonlinear controller design approach based on quasilinear system models. In: Proc. American control conference, San Diego, CA, June 1984, pp 817–824
17. Atherton DP. Nonlinear control engineering. Van Nostrand Reinhold Co., London & New York; full edition 1975, student edition 1982
18. Roppenecker G, O'Reilly J. Parametric output feedback controller design. Automatica 1989; 25(2): 259–265